Journal of Alloys and Compounds 509 (2011) 2555–2561

Contents lists available at ScienceDirect

Journal of Alloys and Compounds

journal homepage: www.elsevier.com/locate/jallcom

Synthesis and characterization of L-carnosine coated iron oxide nanoparticles

Z. Durmus[a], H. Kavas[b], A. Baykal[a,*], H. Sozeri[c], L. Alpsoy[d], S.Ü. Çelik[a], M.S. Toprak[e]

[a] Department of Chemistry, Fatih University, B. Cekmece, 34500 Istanbul, Turkey
[b] Department of Physics, Fatih University, B. Cekmece, 34500 Istanbul, Turkey
[c] TUBITAK-UME, National Metrology Institute, PO Box 54, 41470 Gebze-Kocaeli, Turkey
[d] Department of Biology, Fatih University, B. Cekmece, 34500 Istanbul, Turkey
[e] Department of Functional Materials, Royal Institute of Technology, SE16440 Kista-Stockholm, Sweden

ARTICLE INFO

Article history:
Received 24 September 2010
Received in revised form 7 November 2010
Accepted 11 November 2010
Available online 19 November 2010

Keywords:
Fe_3O_4
Nanocomposites
Surface modification
Amino acid
Magnetic property

ABSTRACT

L-Carnosine coated iron oxide nanoparticles (CCIO NPs) have been prepared via co-precipitation of iron oxide in the presence of L-carnosine. Crystalline phase was identified as magnetite with an average crystallite size of 8 nm as estimated from X-ray line profile fitting. Particle size estimated from TEM by log-normal fitting was ~11 nm. FTIR analysis showed that the binding of carnosine onto the surface of iron oxide is through unidentate linkage of carboxyl group. CCIO NPs showed superparamagnetic charactersitic at room temperature. The magnetic core size of superparamagnetic CCIO NPs was found slightly smaller than the size obtained from TEM, due to the presence of magnetically dead layer. Magnetization measurements revealed that L-carnosine iron oxide composite has immeasurable coercivity and remanence with absence of hysteritic behavior, which implies superparamagnetic behavior at room temperature. The low value of saturation magnetization compared to the bulk magnetite has been explained by spin canting. LDH activity tests showed slight cytotoxicity of high dose of CCIO NPs. The *ac* conductivity of CCIO NPs was found to be greater than that of carnosine and the effective conduction mechanism was found as correlated barrier hopping (CBH). *dc* activation energy of the product at around room temperature was measured as 0.312 eV which was in good agreement with the earlier reports.

1. Introduction

Magnetic nanoparticles are of great interest in recent years due to their technological and clinical applications. Among these, superparamagnetic iron oxide nanoparticles (SPION) receive increasing attention in different fields of physics, medicine, biology, and materials science due to their multifunctional magnetic, catalytic, biological and conducting properties which make them feasible to find applications in various fields [1]. In clinical area, these particles are used as delivery systems for drugs [2], in medical diagnosis [3–5], hyperthermia [6–8], cell separation [9,10], etc. Most of these applications require well-dispersed chemically stable nanoparticles having uniform size and shape. For this reason new technologies in synthesis and methods of analysis have been developed. One of the effective approaches for preventing particle agglomeration is to coat nanoparticles with biocompatible inorganic materials, polymers or other targeting agents. Among the chemicals which may be used for this purpose amino acids are suitable because they play a very important role in the body [11,12]. Proteins, which can provide biocompatibility, high solubility, and hydrophilic properties, are one of the most promising materials among several potential biocompatible and biodegradable substances serving as protective layers on SPION [1].

An important potential application of nano-sized magnetite (NSM) particles is in thermo-genesis, to kill tumor cells under an *ac* magnetic field [3]. To explore their bio-applications the developments of biocompatible, highly water dispersible and functionalized ferromagnetic nano-materials are crucial, asbiomedical applications require chemically stable, well-dispersed and uniform size particles (5–20 nm diameters) [13,14]. Amino acids are highly suitable as ligands for surface modification of NSM particles [11]. Therapy with amino acid imbalance or with amino acids as a dose of nutrients has been widely used to treat cancer sufferers because some amino acids reduced tumor cells. Excess of amino acid, would lead to the tumor cell shrinking or even dying out [1,15,16].

Carnosine, the dipeptide β-alanyl-L-histidine, is found in relatively high concentrations in several body tissues, notably in skeletal muscle, heart muscle and brain, and is the major source of β-alanine in the human body. Although the exact biological role of carnosine is not completely understood, numerous animal studies have demonstrated that it possesses strong and specific antioxidant properties that prevents cell damage, protects against radiation damage, improves heart's function and promotes wound healing. It has also immune boosting properties [17,18]. It has been shown

* Corresponding author.
E-mail address: hbaykal@fatih.edu.tr (A. Baykal).

0925-8388/$ – see front matter © 2010 Elsevier B.V. All rights reserved.
doi:10.1016/j.jallcom.2010.11.088

to be an efficient chelator of copper and other transition metals. Carn is a substrate for the metal-activated enzyme carnosinase and has potential to act as a natural antioxidant in vivo. Some potential medical uses of this peptide have been suggested such as in the treatment of gastric ulcers and inflammations [19].

Magnetic nanoparticles have been surface-modified for the assembly of molecules whose function, when attached, often defines their application. For example, magnetic nanoparticles have been reported in magnetofection and drug delivery as well as in bio-sensing by attaching molecules including chemicals, oligonucleotides, and proteins [20,21].

To our knowledge, only few studies about the capping of the amino acids on the surface of the magnetic nanoparticles were realized [15,22]. In a recent worked we reported on the a spontaneous, single-step synthesis of magnetic nanoparticulate spheres using a combination poly-L-lysine, L-histidine and iron oxide nanoparticles [23–25]. In this study, we focus on a new synthesis route to prepare amino acid modified iron oxide in one step and report physicochemical properties of these composite nanomaterial.

2. Experimental

2.1. Synthesis

All chemicals ($FeCl_3{\cdot}2H_2O$, $FeCl_2{\cdot}4H_2O$, L-carnosine) were obtained from Merck and used without further purification. To an aqueous solution of a mixture of Fe(III) and Fe(II) salts, L-carnosine solution in the molar ratio 2Fe(III):1Fe(II):4 L-carnosine was added and kept at a constant temperature of 40 °C for 15 min under vigorous stirring. Then a solution of ammonium hydroxide was added till the pH was raised to ~11 at which a black suspension was formed. This suspension was then refluxed at 80 °C for 6 h, under vigorous stirring and Ar gas. L-Carnosine coated iron oxide nanoparticles (CCIO NPs) were separated from the aqueous solution by magnetic decantation, washed with distilled water several times and then dried in an oven overnight.

2.2. Instrumentations and analytical techniques

X-ray powder diffraction (XRD) analysis was conducted on a Rigaku Smart Lab Diffractometer operated at 40 kV and 35 mA using Cu Kα radiation.

Transmission electron microscopy (TEM) analysis was performed using a FEI Tecnai G2 Sphera microscope. A drop of diluted sample in alcohol was dripped on a TEM grid.

Fourier transform infrared (FT-IR) spectra were recorded in transmission mode with a Perkin Elmer BX FT-IR infrared spectrometer. The powder samples were ground with KBr and compressed into a pellet. FTIR spectra in the range 4000–400 cm^{-1} were recorded in order to investigate the nature of the chemical bonds formed.

The real (ε') and imaginary (ε'') parts of complex dielectric permittivity $\varepsilon^*[=\varepsilon'(\omega)+i\varepsilon''(\omega)]$ were measured with a Novocontrol dielectric-impedance analyzer. The dielectric data (ε', ε'') were collected as a function of temperature and frequency. The films were sandwiched between gold blocking electrodes and the conductivities were measured in the frequency range 0.1 Hz to 3 MHz at 10 °C intervals. The temperature was controlled with a Novocontrol cryosystem, which is applicable between 20 and 120 °C.

VSM measurements were performed by using a Vibrating sample magnetometer (LDJ Electronics Inc., Model 9600). The magnetization measurements were carried out in an extenal field up to 15 kOe at room temperature.

The thermal stability was determined by thermogravimetric analysis (TGA, Perkin Elmer Instruments model, STA 6000). The TGA thermograms were recorded for 5 mg of powder sample at a heating rate of 10 °C/min in the temperature range of 30–800 °C under nitrogen atmosphere.

Lactate dehydrogenase (LDH) kit was purchased from Roche (Basel, Switzerland). Fetal bovine serum (sigma), RPMI-1640, penicillin/streptomycin, and L-glutamine were purchased from Invitrogen (Paisley, UK).

The human lymphocyte cells were isolated from heparinized blood samples by density-gradient centrifugation over Histopaque washed twice with RPMI-1640 and resuspended in RPMI-1640 supplemented with 5% human AB serum, 100 U/ml penicillin/streptomycin and 2 mM L-glutamine.

Cellular injury was determined by measuring the LDH released into the cell culture medium. LDH was assayed by measuring the increase of NADH absorbance at 490 nm at 25 °C, using an Biotek Power Wave XS mode Elisa Reader (Unico, NJ, USA). Human lymphocyte cells at 2×10^5/ml were treated with 1, 5, 10 and 20 mM L-carnosine and L-carnosine coated iron oxide NPs for 24 h, 48 h and 72 h at 37 °C in 5% CO_2. Then, LDH activity released from human lymphocyte cells into the culture medium, which represents cell death, was determined with an LDH kit as described previously [26,27]. Triton X 100 was used as a positive control.

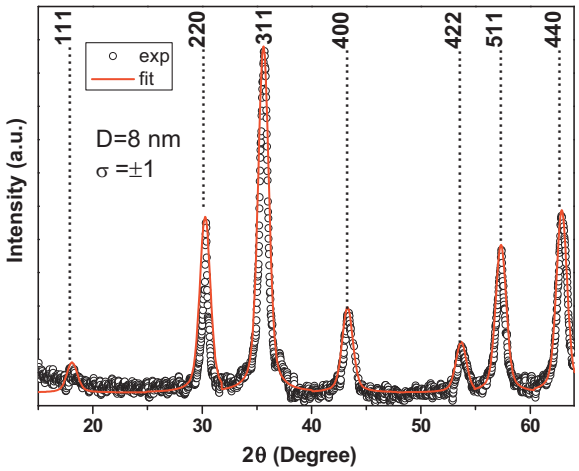

Fig. 1. XRD pattern and line profile fitting of CCIO NPs.

3. Results and discussion

3.1. XRD analysis

Phase investigation of the crystalline product was performed by XRD and the diffraction pattern is presented in Fig. 1. The XRD pattern indicates that the product consists of magnetite, Fe_3O_4, and the diffraction peaks are broadened owing to very small crystallite size. All of the observed diffraction peaks are indexed by the cubic structure of Fe_3O_4 (JCPDS no. 19-629) revealing a high phase purity of magnetite. The following reaction was suggested for the formation of magnetite [25]:

$$Fe^{2+}{}_{(aq)} + 2Fe^{3+}{}_{(aq)} + 8OH^-{}_{(aq)} \rightarrow Fe_3O_{4(s)} + 4H_2O$$

The mean size of the crystallites was estimated from the diffraction pattern by line profile fitting method using Eq. (1) given in Refs. [28,29]. The line profile, shown in Fig. 1 was fitted for observed six peaks with the following miller indices: (1 1 1), (2 2 0), (3 1 1), (4 0 0), (4 2 2), (5 1 1), and (4 4 0). The average crystallite size, D and σ, was obtained as 8 ± 2 nm as a result of this line profile fitting.

3.2. FTIR analysis

FTIR spectra of iron oxide, carnosine, CCIO NPs and suggested linkage of carnosine to iron oxide surface are given in Fig. 2a–c. The presence of the iron oxide nanoparticles evidenced by the strong absorbtion bands at around 570–590 cm^{-1} that confirm the metal-oxygen streching are presented in Fig. 2a and b [25,30–32].

In the spectrum of pure carnosine (Fig. 2c) the characteristic ν_{NH_2} stretching frequency of carnosine is observed at ~3240 cm^{-1} (which overlaps with the broad OH peak coming from H_2O), and asymmetric and symmetric stretching frequencies of carboxylate (COO^-) are observed at 1568 cm^{-1} $\nu_{as}(COO^-)$ and 1404 cm^{-1} $\nu_s(COO^-)$, respectively. The peaks at 2850 and 2785 cm^{-1} for symmetric and asymmetric stretching vibrations of C–H groups. The absorption band at1636 cm^{-1} is due to absorbed water for pure carnosine (Fig. 2c) and for nanocomposite (Fig. 2b) [18]. In the spectrum for CCIO NPs (Fig. 2b), the band due to ν_{as} COO^- cannot be unequivocally identified because it overlaps with the C=C stretching vibration of the imidazole ring (1590–1570 cm^{-1}). $\nu_s(COO^-)$ of pure carnosine shifted from 1404 to 1390 cm^{-1} in CCIO NPs. Moreover, a strong IR band due to the $\delta(COO^-)$ mode was observed at 628 cm^{-1} [15,18,23,33–37]. The spectral behavior of the so-called amide I band, which is essentially the C=O stretching vibration of the amide group, appears somewhat unexpected as it shows an important displacement to lower energies in the complex, although

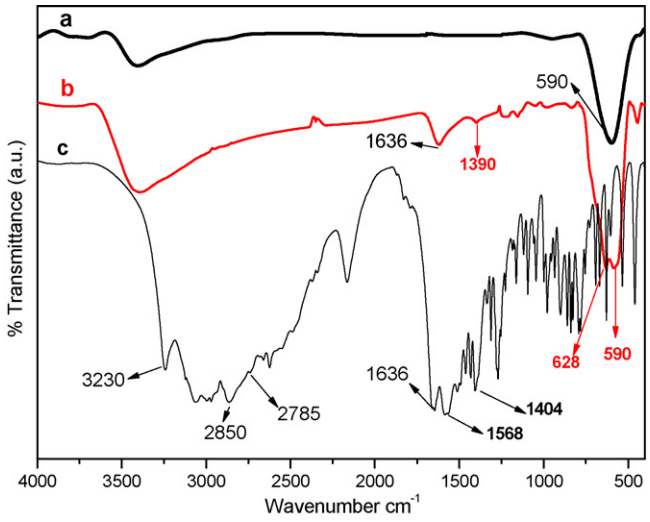

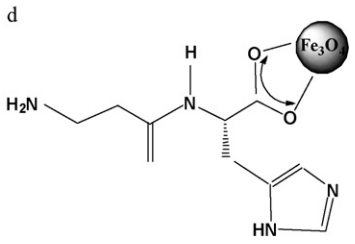

Fig. 2. FTIR spectra of (a) iron oxide, (b) CCIO NPs, (c) carnosine, and (d) suggested linkage of carnosine to iron oxide surface.

this carbonyl group is not directly involved in coordination. Nevertheless, as explained by Freeman and Szymanski [38] peptide groups whose N-atoms are involved in metal binding have much more longer C=O and shorter C–N bonds than free peptides [18,38]. In the FT-IR spectra of CCIO NPs, metal-N stretching (~470 cm^{-1}) was not observed.

According to these results, FTIR analyses suggest that L-carnosine remains chemisorbed on the surface of iron oxide (Fig. 2d) via carboxyl groups (C=O).

3.3. TGA analysis

TGA thermograms of iron oxide (Fe_3O_4), L-carnosine and CCIO NPs are presented in Fig. 3, which can be used for a quantitative comparison of degradation behavior of different samples. Iron oxide shows no weight loss in the temperature range of TG analysis. On the other hand, degradation is seen in the TGA curves of both carnosine and CCIO NPs samples. Combustion of L-carnosine is not completed within the temperature interval of analysis. CCIO NPs shows a slight weight loss, while carnosine exhibits a considerable thermal stability up to 240 °C. Degradation of L-carnosine over the iron oxide begins at a much lower temperature. This behavior could be originated from the fact that iron oxide particles behave as catalysts thus reducing the degradation temperature of carnosine. Based on the thermogram, carnosine is 10% of the CCIO NPs, which means an inorganic content is about 90%.

3.4. TEM analysis

Morphology and size distribution of CCIO NPs were analyzed using TEM. Few micrographs at different magnifications, a histogram calculated thereof and an SAED pattern are presented in

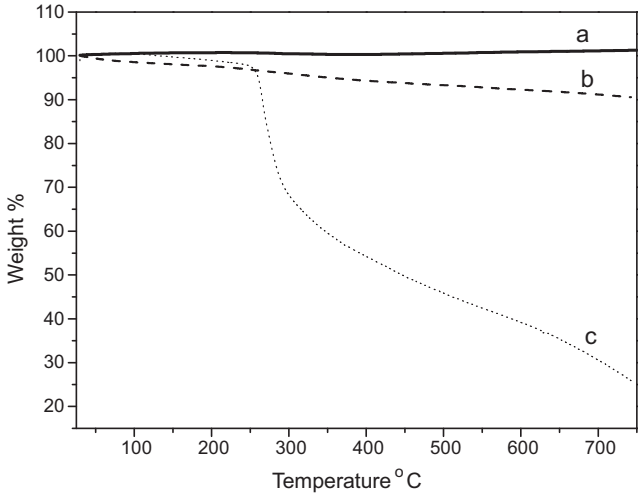

Fig. 3. TGA thermograms of (a) iron oxide, (b) CCIO NPs, and (c) L-carnosine.

Fig. 4. Fe_3O_4 particles exhibit near spherical morphology. SAED pattern of CCIO NPs is given in the inset of Fig. 4c which is typical of polycrystalline nanoparticles. Average particle size was calculated by log-normal fitting to the size distribution histogram and was obtained as 11.5 ± 0.5 nm. As compared with the crystallite size obtained from X-ray line profile fitting, this reflects nearly single crystalline nature of the CCIO NPs.

3.5. Room temperature VSM analysis

Magnetization measurements of CCIO NPs were performed using VSM technique and results at 300 K are shown in Fig. 5. The magnetization increases with increasing external magnetic field strength, however, it did not reach the saturation state yet at a high magnetic field of 15 kOe. The saturation magnetization (*Ms* calculated from a plot of *M* vs. $1/H$ (M at $1/H \geq 0$)) value of experimental curve as 67 emu/g (347 emu/cm^3) at room temperature and also it is verified by the log normal weighted Langevien fit of this curve. These values are comparatively lower than that of bulk magnetite with an *Ms* of 92 emu/g (480–500 emu/cm^3) [39–41].

There are several interpretations to explain reduced *Ms* in the literature. For instance, formation of dead surface on magnetite core is one of them. Maghemite shell having lower magnetization compared to magnetite can be formed on a magnetite core via oxidation reactions [42]. Then, total saturation magnetization decreases and can be determined by core-surface model. Another interpretation is canting of the surface spins due to the antiferromagnetic interactions. Later works showed that spin canting is not a surface but a finite size effect which is uniform through the whole volume of the particle [43,44]. Very recently, it was shown that coating magnetite with oleic acid did not decrease the saturation magnetization which means that spin canting was not observed [45]. This works reveals that it is possible to coat magnetite NPs without spin canting and high saturation magnetization values, close to the theoretical value, can be obtained. To explain reduced *Ms* in L-carnosine coated samples, we think that FTIR measurements give us very useful hint. We have observed that L-carnosine is bound to magnetite via carboxyl groups (C=O). In this process, some of the free electrons of oxygen atoms which play very important role in the strength of super exchange interaction between Fe–O–Fe atoms are used by carbon atoms. As a result, super exchange interaction weakens and total magnetization of the composite decreases. Chemisorption of the oxygen atoms distorts the surface spin structure and, thus, we think that spin canting effect is more reasonable interpretation.

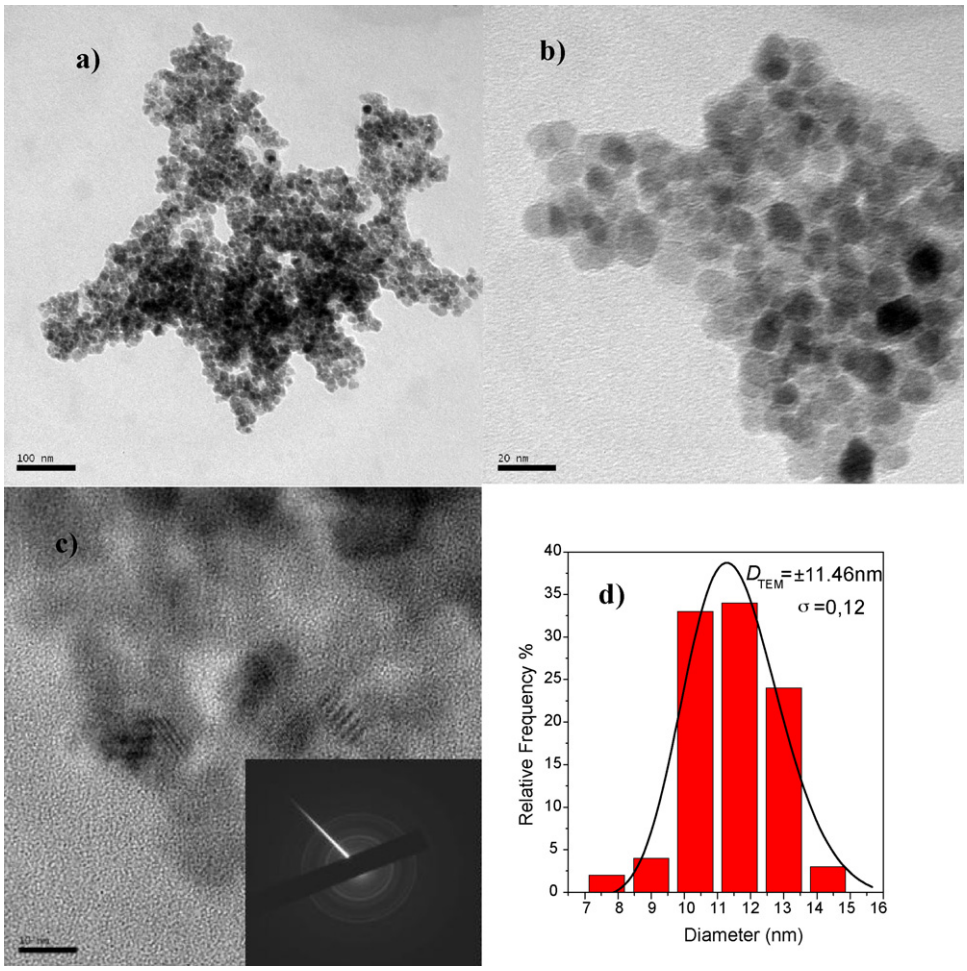

Fig. 4. (a–c) TEM micrographs of CCIO NPs at different magnifications, inset the SAED pattern; and (d) calculated histogram from several TEM images with log-normal fitting.

The RT hysteresis curve is well fitted with the log normal weighted Langevien function [46]:

$$M(H, D) = \sum M_i V_i f(d_i) L(x_i) \quad (1)$$

where M_i and V_i are magnetization and volume of ith particle, respectively. And $f(d_i)$ is log-normal size distribution function and $L(x_i)$ is the Langevien function. The details and calculation of the mean diameter of NP can be found in our previous study [46]. The fitting parameters $d_m = 7.9$ nm, $\sigma = 0.75$ and the calculated average diameter $D_m = 8.94$ nm are obtained by fitting curve. Magnetic core size obtained for iron oxide from the fitting is slightly smaller than the size obtained from TEM and X-ray line profile fitting due to the presence of magnetically dead layer on the nanoparticle surface. This also confirms nearly single crystalline character of iron oxide NPs.

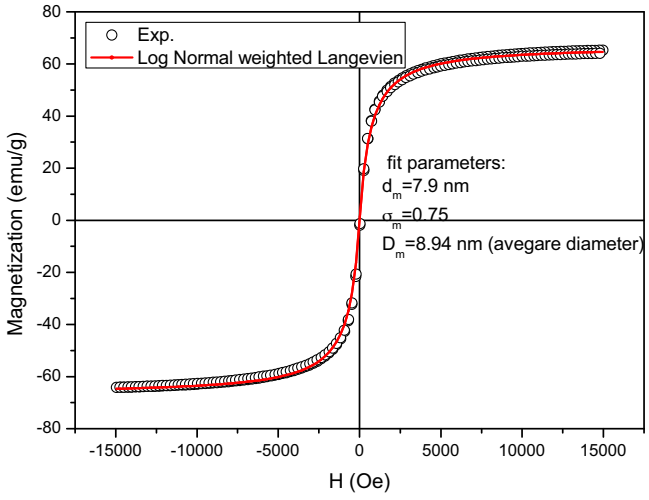

Fig. 5. M vs. H curves at room temperature and their log-normal size weighted Langevien fit of carnosine coated iron oxide NPs.

3.6. Temperature and frequency dependent conductivity and dielectric permittivity measurements

The ferrites have semiconducting characteristic in the frequency range of 1–3 MHz. So the total measured conductivity σ_T consists of two terms: $\sigma_T = \sigma_{dc}(T) + \sigma(\omega)$ [47]. The first one is the σ_{dc}, dc electrical conductivity $L(x_i)$ which is related to the drift of electric charge carriers via band conduction mechanism and is temperature-dependent by following an Arrhenius relation: $\sigma_{dc} = \sigma_0 + \exp(-E_a/kT)$. The second term, $\sigma(\omega)$, is frequency-dependent. $\sigma(\omega)$ is related to the dielectric relaxation caused by the localized electric charge carriers and obeys the empirical formula of frequency dependence given by ac power law [48]

$$\sigma = B(T)w^{n(T)} \quad (2)$$

where $B(T)$ and $n(T) \leq 1$ are constants at a certain temperature. Temperature dependency of n helps the type of conduction mechanism. In brief, conduction due to small polarons (SP) are usually

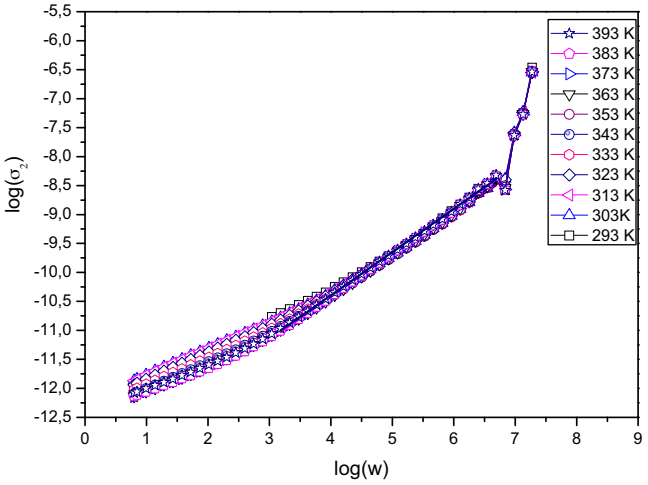

Fig. 6. $\log(\sigma_2)$ vs. $\log(\omega)$ for carnosine at various temperatures and their fit.

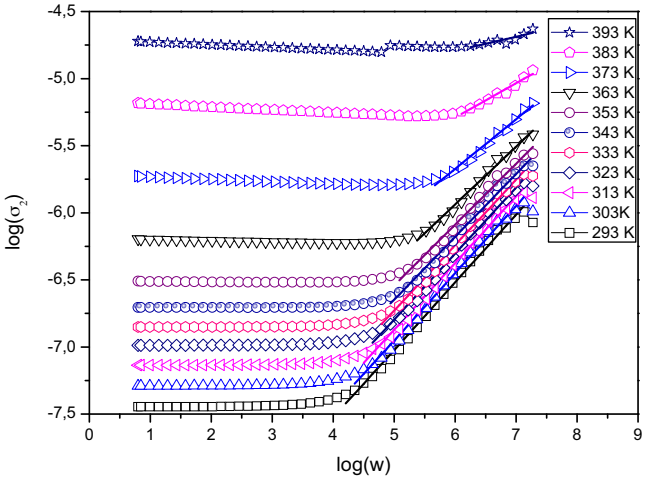

Fig. 7. $\log(\sigma_2)$ vs. $\log(\omega)$ for CCIO NPs at various temperatures and their fit.

associated with increase in n with increasing temperature, while conduction due to correlated barrier hopping (CBH) shows a decrease in n with increasing temperature. Overlap large polarons (OLP) show a linearly decreasing of n with temperature reaching a minimum then start to increase again [48].

The angular frequency dependent *ac* conductivity curves at different temperatures are shown in Figs. 6 and 7 for L-carnosine and CCIO NPs, respectively. The conductivity of L-carnosine increases

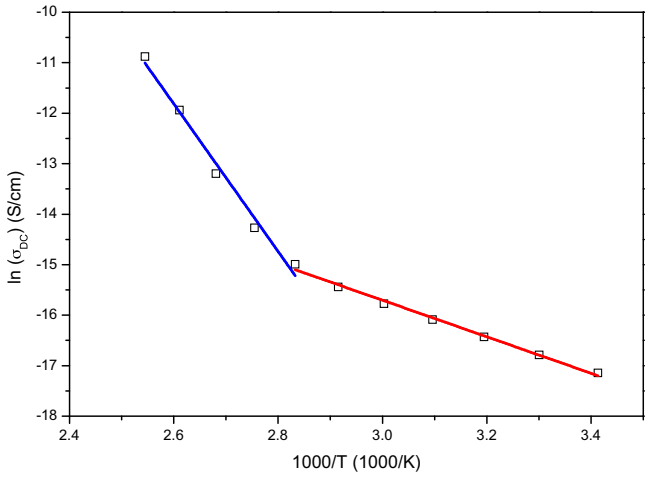

Fig. 8. $\log(\sigma_{dc})$ vs. $1000/T$ for CCIO NPs.

with increasing temperature linearly independent of temperature at higher frequencies while it is slightly temperature dependent at low frequencies. The CCIO NPs first show frequency independent conductivity at low frequencies which increase linearly above 4 Hz by increasing frequency. It is also found to be temperature dependent. The conductivity of CCIO is in the order of 10^{-4}–10^{-8} while that of L-carnosine is in the order of 10^{-7}–10^{-12}, so it can be inferred that L-carnosine behaves as insulating interparticle interface.

The σ_{dc} values are found by extrapolation of frequency independent part of (lower frequency regimes) curves to the zero frequency. Fig. 8 shows the variation of σ_{dc} conductivity with respect to temperature. The σ_{dc} conductivity curve has two different slopes and so it is fitted for two different regimes according to the Arrhenius law. The ΔE are found as 0.312 eV for low temperature (LT) region and 1.26 eV for high temperature (HT) region. The results are consistent with the results for L-lysine coated iron oxide NP reported as 0.22–0.43 eV [23]. Details of the effect of various parameters such as porosity, chemical composition, particle size [49,50] and cation distribution [51] on the conductivity of ferrites have been explained in detail in earlier reports.

The linearly temperature dependent *ac* conductivity regimes (higher frequency regime) are fitted by Eq. (1) and are shown by solid lines to determine the conduction mechanism. The obtained *n* and *B* values at various temperatures are shown in Fig. 9. While the *n* of L-carnosine remains constant about 0.75, the *n* of CCIO NPs slightly decrease from 0.5 till 360 K, then decrease sharply reaching 0.1 at HT. So the effective conduction mechanism is found as correlated barrier hopping (CBH) which has a characteristic of decreasing *n* with increasing temperature.

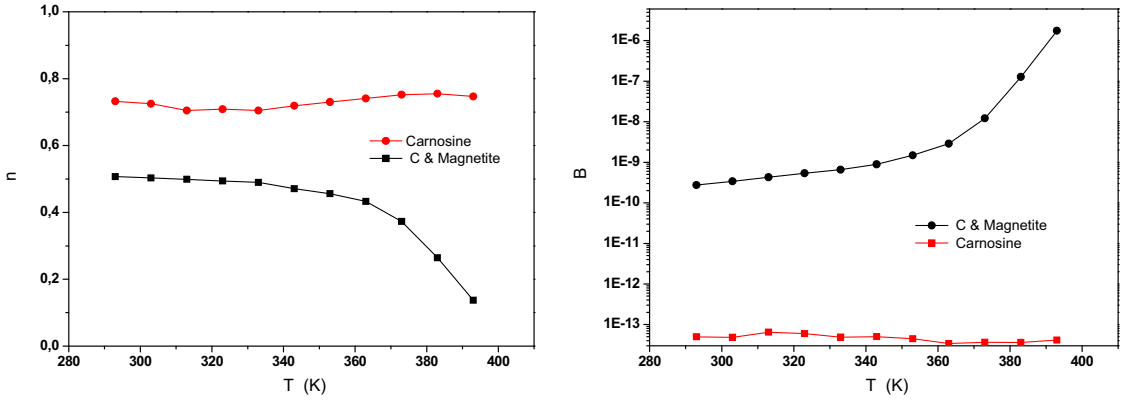

Fig. 9. The fit parameters of *n* and *B* for carnosine and CCIO NPs.

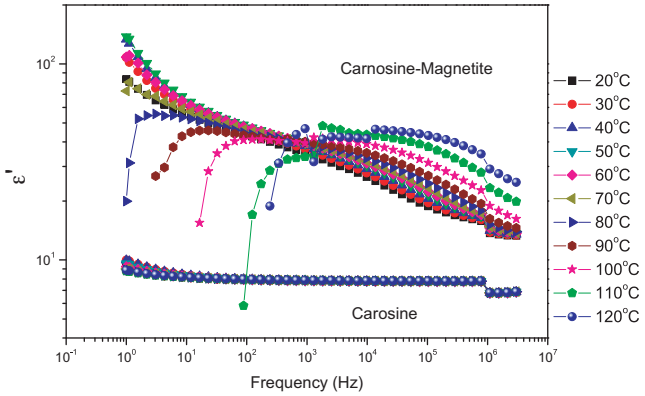

Fig. 10. Plots of ε' vs. frequency of L-carnosine and CCIO NPs at various temperatures.

Fig. 10 shows the ε' as a function of frequency in the temperature range of 20–120 °C for both carnosine and CCIO NPs samples. While the ε' does not change for L-carnosine with temperature and frequency, it is strongly frequency and temperature dependent for CCIO NPs. At higher frequencies the ε' of CCIO NPs decreases by increasing frequency.

Fig. 11 shows the ε'' as a function of frequency for L-carnosine and CCIO NPs samples in the temperature range of 20–120 K. While the ε'' slightly decrease by frequency for L-carnosine, it decreases sharply for CCIO NPs. ε'' in CCIO NPs has slight temperature dependence at lower frequencies but this dependency becomes weak at higher frequencies which can be explained by Koop's theory, based on the Maxwell–Wagner model for the homogeneous double structure [52] in which the highly conducting grains are separated by relatively poor conducting grain boundaries and are found to be more effective at higher frequencies, while the conducting grains are more effective at lower frequencies [53]. The conductivity difference between grains and grain boundaries means different resistances causing the accumulation of charge carriers in separated boundaries and increase in dielectric constants. The polarization in ferrites is through a mechanism similar to the conduction process by electron exchange between Fe^{2+} and Fe^{3+}, the local displacement of electrons in the direction of the applied field occurs and these electrons determine the polarization. At higher frequencies and LT, the polarization decreases and becomes slightly temperature and frequency dependent due to the electron exchange between Fe^{2+} and Fe^{3+} cannot follow the alternating field. Previously, the sharp changes in dielectric constant at lower frequency was attributed to the predominance of species like Fe^{2+} ions, oxygen vacancies, grain boundary defects, etc. [54]. The decrease in dielectric constant with frequency is natural

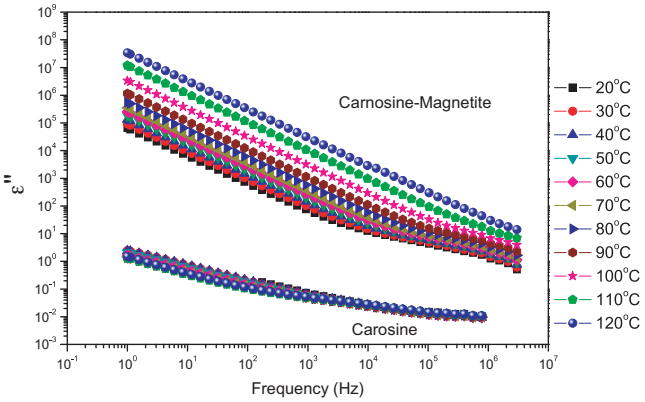

Fig. 11. Plots of ε'' vs. frequency of L-carnosine and CCIO NPs at various temperatures.

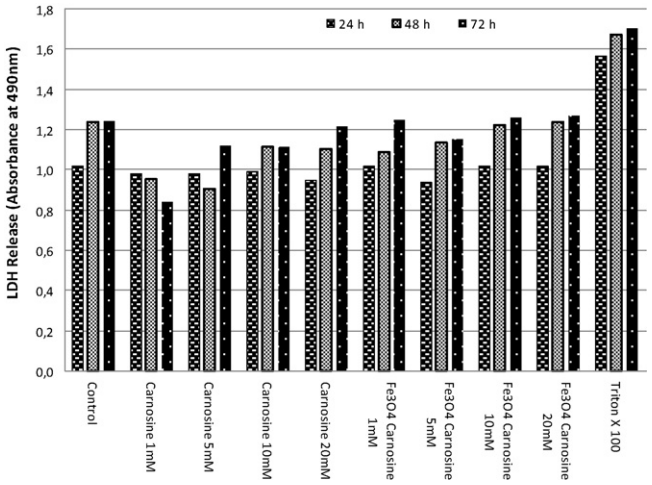

Fig. 12. LDH activity test results for various doses of carnosine, CCIO NPs, positive and negative controls after 24 h, 48 h and 72 h incubation time period.

because of the fact that any species contributing to polarization is found to show lagging behind the applied field at higher and higher frequencies [55]. The dielectric constants increase with increasing temperature as seen in semiconductors. Thermal energy converts the bound charges to the charge carriers, and increasing charge carrier concentration always gives easy alignment of dipoles in the applied *ac* electrical field and therefore resulting in increase of dielectric constants.

3.7. Toxicity

L-Carnosine protects the cell against several negative effects because of these features. LDH activity released from human lymphocyte cells into the culture medium, which is a direct representation of cell death, was determined and results are presented in Fig. 12. Various concentrations of carnosine tested at three different durations as 24 h, 48 h and 72 h did not show any cytotoxicity. Although samples of CCIO NPs did not show any cytotoxicity after 24 and 48 h incubations, sonar analysis performed after exposure to 10 mM and 20 mM CCIO NPs for 72 h showed some cytotoxic effects. This cytotoxic effect is very low according to the test kit used (4%). Induction in the level of LDH were found insignificant in 10 mM and 20 mM CCIO NPs for 72 h group when compared with the control by using ANOVA statistics test (SPSS 15 software) ($p < 0.7$).

4. Conclusions

We have successfully synthesized L-carnosine coated iron oxide nanoparticles and characterized it in detail for composition, microstructure, *ac–dc* conductivity performance, and dielectric permittivity. L-carnosine is assessed to be covalently bonded to the iron oxide nanoparticle surface. The magnetic core size of superparamagnetic CCIO NPs was found slightly smaller than the size obtained from TEM, which reveals a core–shell type of structure due to the magnetically dead layer. The reduced saturation magnetization of the nanocomposite was explained by spin canting. The *ac* conductivity of CCIO NPs is found to be greater than that of L-carnosine. The power law analysis of *ac* conductivity shows the effective conductivity mechanism in composite is correlated barrier hopping (CBH) based conduction. The *dc* activation energy at around room temperature is found as 0.312 eV consistent with earlier reports.

The synthesized amino acid-coated magnetic nanoparticles might be applied to cell separation, diagnosis and targeted drug delivery for cancer therapy. In addition, the synthetic process pre-

sented here may have potential applications to synthesize other amino acid capped nanoparticle configurations, including essential amino acids and some proteins coating.

Acknowledgements

The authors are thankful to the Fatih University, Research Project Foundation (Contract Nos. P50020902-2 and P50030905-2) and Turkish Ministry of Industry and Trade (Contract No. 00185.STZ.2007-2) for financial support of this study. MST acknowledges the fellowship from Knut and Alice Wallenbergs Foundation (No. UAW2004.0224).

References

[1] J. Wang, Y. Sun, L. Wang, X. Zhu, H. Zhang, D. Song, Colloids Surf. B: Biointerfaces 81 (2010) 600.
[2] L.D. Tran, N.T. Hoang, T.T. Mai, H.V. Tran, N.T. Nguyen, T.D. Tran, M.H. Do, Q.T. Nguyen, D.G. Pham, T.P. Ha, H.V. Le, P.X. Nguyen, S. Liu, Colloids Surf. A: Physicochem. Eng. Aspects 371 (2010) 104.
[3] Q. Wei, Z. Xiang, J. He, G. Wang, H. Li, Z. Qian, M. Yang, Biosens. Bioelectron. 26 (2010) 627.
[4] G. Li, Y. Jiang, K. Huang, P. Ding, J. Chen, J. Alloys Compd. 466 (2008) 451.
[5] Q. Wei, T. Li, G. Wang, H. Li, Z. Qian, M. Yang, Biomaterials 31 (2010) 7332.
[6] J. Qu, G. Liu, Y. Wang, R. Hong, Adv. Powder Technol. 21 (2010) 461.
[7] D. Zhao, X.W. Zeng, Q.S. Xi, J.T. Tang, J. Alloys Compd. 469 (2009) 215.
[8] D.L. Zhao, X.X. Wang, X.W. Zeng, Q.S. Xia, J.T. Tang, J. Alloys Compd. 477 (2009) 739.
[9] W. Zhou, W. He, S. Zhong, Y. Wang, H. Zhao, Z. Li, S. Yan, J. Magn. Magn. Mater. 321 (2009) 1025.
[10] M. Zhao, X. Zhang, S. Wang, C. Chen, Y. Cui, J. Med. Colleges PLA 24 (2009) 239.
[11] D.C. Culita, G. Marinescu, L. Patron, O. Carp, C.B. Cizmas, L. Diamandescu, Mater. Chem. Phys. 15 (2008) 381.
[12] C. Vogt, M.S. Toprak, M. Muhammed, S. Laurent, J.-L. Bridot, R.N. Mueller, J. Nanopart. Res. 12 (2010) 1137.
[13] C.C. Berry, J. Mater. Chem. 15 (2005) 543.
[14] D. Patel, Y. Chang, G. Lee, Curr. Appl. Phys. 9 (2009) S32.
[15] S.L. Tie, Y.Q. Lin, H.C. Lee, Y.S. Bae, C.H. Lee, Colloids Surf. A: Physicochem. Eng. Aspects 273 (2006) 75.
[16] G. Marinescu, L. Patron, D.C. Culita, C. Neagoe, C.I. Lepadatu, I. Balint, L. Bessais, C.B. Cizmas, J. Nanopart. Res. 8 (2006) 1045.
[17] S. Thomas, N. Biswas, V.V. Malkar, T. Mukherjee, S. Kapoor, Chem. Phys. Lett. 491 (2010) 59.
[18] C.C. Wagner, E.J. Baran, J. Raman Spectrosc. 39 (2008) 474.
[19] A. Peterson, N. Nguyen, H. i Okamoto, A.S. Giraud, I.R. van Driel, L.M. Judd, Regul. Pept. 160 (2010) 9.
[20] Y.H. Ma, J. Biomater, Sci. Polym. Ed. 15 (8) (2004) 1033.
[21] B.G. Nidumolu, Biotechnol. Prog. 22 (1) (2006) 91.
[22] D. Patel, Y.G. Chang, H. Lee, Anal. Biochem. 388 (1) (2009) 81.
[23] M.S. Toprak, B.J. McKenna, M. Mikhaylova, J.H. Waite, G.D. Stucky, Adv. Mater. 19 (2007) 1362.
[24] B. Ünal, Z. Durmus, A. Baykal, H. Sözeri, M.S. Toprak, L. Alpsoy, J. Alloys Compd. 505 (2010) 172.
[25] Z. Durmus, H. Kavas, M.S. Toprak, A. Baykal, T.G. Altıncekic, A. Aslan, A. Bozkurt, S. Cosgun, J. Alloys Compd. 484 (2009) 371.
[26] Q. Li, M. Kobayashi, T. Kawada, Toxicology 255 (2009) 53.
[27] K. Yao, D. Huang, B. Xu, N. Wang, Y. Wang, S. Bi, Analyst 135 (2010) 116.
[28] T. Wejrzanowski, R. Pielaszek, A. Opalińska, H. Matysiak, W. Lojkowski, K.J. Kurzydlowski, Appl. Surf. Sci. 253 (2006) 204.
[29] R. Pielaszek, in: Proceedings of the XIX Conference, Krakow, Poland, Appl. Crystallogr. 43 (2003).
[30] L.J. Kirwan, P.D. Fawell, W.V. Bronswijk, Langmuir 19 (2003) 5802.
[31] Z. Durmus, Master Thesis, Fatih Univ., Istanbul-Turkey, 2009.
[32] T. Özkaya, M.S. Toprak, A. Baykal, H. Kavas, Y. Köseoğlu, B. Aktaş, J. Alloys Compd. 472 (2009) 18.
[33] E. Torreggiaıni, M. Tamba, G. Fini, Bioploymers 57 (2000) 149.
[34] A. Torreggiani, P. Taddei, A. Tinti, G. Fini, J. Mol. Struct. 64 (2002) 61.
[35] B. Unal, Z. Durmus, H. Kavas, A. Baykal, M.S. Toprak, Mater. Chem. Phys. 123 (2010) 184.
[36] K. Nakamoto, Infrared and Raman Spectra of Inorganic and Coordination Compounds, Part B, 5th ed., Wiley, New York, 1997.
[37] S. Tie, Y. Lin, H. Lee, Y. bae, C. Lee, Colloids Surf. A: Physicochem. Eng. Aspects 273 (2006) 75.
[38] H.C. Freeman, J.T. Szymanski, Acta Crystallogr. 22 (1967) 22.
[39] D.H. Han, J.P. Wang, H.L. Luo, J. Magn. Magn. Mater. 136 (1994) 176.
[40] S. Chikazumi, Physics of Ferromagnetism, 2nd ed., Clarendon Press, Oxford, 1997.
[41] E. Blum, A. Cebers, M.M. Maiorov, Magnetic Fluids, Walter de Gruyter, Berlin, 1997.
[42] F. Bodeker, S. Morup, S. Linderoth, Phys. Rev. Lett. 72 (1994) 282.
[43] Q.A. Pankhurst, R.J. Pollard, Phys. Rev. Lett. 67 (2) (1991) 248.
[44] F.T. Parker, M.W. Foster, D.T. Margulies, A.E. Berkowitz, Phys. Rev. B 47 (13) (1993) 7885.
[45] A.G. Roca, D. Niznansky, J. Poltierova-Vejpravova, B. Bittova, M.A. González-Fernández, C.J. Serna, M.P. Morales, J. Appl. Phys. 105 (2009) 114309.
[46] H. Kavas, A. Baykal, M.S. Toprak, Y. Koseoglu, M. Sertkol, B. Aktas, J. Alloys Compd. 479 (2009) 49.
[47] A. Ghosh, Phys. Rev. B 42 (2) (1990) 1388.
[48] S.R. Elliott, Adv. Phys. 36 (1987) 135.
[49] E.J.W. Verway, P.W. Haayman, Physica 8 (1941) 979.
[50] V.L.G. Uitert, Proc. IRE, vol. 44, 1956, p. 1294.
[51] R.K. Puri, V. Sayen, Proc. ICF-5, India, 1989, p. 245.
[52] A.M.M. Farea, S. Kumar, K.M. Batoo, J. Alloys Compd. 464 (2008) 361.
[53] K.M. Batoo, S. Kumar, C.G. Lee, Curr. Appl. Phys. 9 (2009) 1397.
[54] J.C. Maxwell, Electric and Magnetism, Oxford University Press, New York, 1973, p. 828.
[55] I.H. Gul, A.Z. Abbasi, F. Amin, M. Anis-ur-Rehman, A. Maqsood, J. Magn. Magn. Mater. 311 (2007) 494.